Fudamoto, Y, Oesch, PA, Walter, F, Decarli, R, Carilli, CL, Ferrara, A, Barrufet, L, Bouwens, R, Dessauges-Zavadsky, M, Nelson, EJ, Dannerbauer, H, Illingworth, G, Inoue, AK, Marques-Chaves, R, Perez-Fournon, I, Riechers, DA, Schaerer, D, Smit, R, Sugahara, Y and Van Der Werf, P

The NOEMA observations of GN-z11: Constraining the neutral interstellar medium and dust formation in the heart of cosmic reionization at z = 10.6

Monthly Notices of the ROYAL ASTRONOMICAL SOCIETY

MNRAS **530,** 340–346 (2024) https://doi.org/10.1093/mnras/stae556
Advance Access publication 2024 February 22

The NOEMA observations of GN-z11: constraining the neutral interstellar medium and dust formation in the heart of cosmic reionization at $z = 10.6$

Y. Fudamoto [1,2,3]★ P. A. Oesch [4,5] F. Walter,[6] R. Decarli [7] C. L. Carilli,[8] A. Ferrara,[9] L. Barrufet [4] R. Bouwens,[10] M. Dessauges-Zavadsky [4] E. J. Nelson,[11] H. Dannerbauer,[12] G. Illingworth,[13] A. K. Inoue [2,14] R. Marques-Chaves,[4] I. Pérez-Fournon,[12,15] D. A. Riechers,[16] D. Schaerer,[4] R. Smit,[17] Y. Sugahara[2,3] and P. van der Werf[18]

[1] *Center for Frontier Science, Chiba University, 1-33 Yayoi-cho, Inage-ku, Chiba 263-8522, Japan*
[2] *Waseda Research Institute for Science and Engineering, Faculty of Science and Engineering, Waseda University, 3-4-1 Okubo, Shinjuku, Tokyo 169-8555, Japan*
[3] *National Astronomical Observatory of Japan, 2-21-1, Osawa, Mitaka, Tokyo, Japan*
[4] *Department of Astronomy, University of Geneva, Chemin Pegasi 51, CH-1290 Versoix, Switzerland*
[5] *Cosmic Dawn Center (DAWN), Niels Bohr Institute, University of Copenhagen, Jagtvej 128, København N, DK-2200, Denmark*
[6] *Max Planck Institute for Astronomy, Königstuhl 17, D-69117 Heidelberg, Germany*
[7] *INAF – Osservatorio di Astrofisica e Scienza dello Spazio di Bologna, via Gobetti 93/3, I-40129 Bologna, Italy*
[8] *National Radio Astronomy Observatory, P. O. Box 0, Socorro, NM 87801, USA*
[9] *Scuola Normale Superiore, Piazza dei Cavalieri 7, I-50126 Pisa, Italy*
[10] *Leiden Observatory, Leiden University, NL-2300 RA Leiden, the Netherlands*
[11] *Department for Astrophysical and Planetary Science, University of Colorado, Boulder, CO 80309, USA*
[12] *Instituto de Astrofísica de Canarias (IAC), E-38205 La Laguna, Tenerife, Spain*
[13] *Department of Astronomy and Astrophysics, University of California, Santa Cruz, CA 95064, USA*
[14] *Department of Physics, School of Advanced Science and Engineering, Faculty of Science and Engineering, Waseda University, 3-4-1, Okubo, Shinjuku, Tokyo 169-8555, Japan*
[15] *Dpto. Astrofísica, Universidad de la Laguna, E-38206 La Laguna, Tenerife, Spain*
[16] *I. Physikalisches Institut, Universität zu Köln, Zülpicher Strasse 77, D-50937 Köln, Germany*
[17] *Astrophysics Research Institute, Liverpool John Moores University, 146 Brownlow Hill, Liverpool L3 5RF, United Kingdom*
[18] *Leiden Observatory, Leiden University, P.O. Box 9513, NL-2300 RA Leiden, the Netherlands*

Accepted 2024 February 13. Received 2024 January 23; in original form 2023 September 2

ABSTRACT

We present results of dust continuum and [C II] 158 μm emission line observations of a remarkably UV luminous ($M_{\rm UV}$ = −21.6) galaxy at $z = 10.603$: GN-z11. Using the Northern Extended Millimeter Array (NOEMA), observations have been carried out over multiple observing cycles. We achieved a high sensitivity resulting in a $\lambda_{\rm rest} = 160\,\mu$m continuum 1 σ sensitivity of 13.0 μJy beam^{-1} and a [C II] emission line 1 σ sensitivity of 31 mJy beam^{-1} km s^{-1} using 50 km s^{-1} binning with a $\sim$ 2 arcsec synthesized beam. Neither dust continuum nor [C II] 158 μm line emission are detected at the expected frequency of $\nu_{\rm [C\,II]} = 163.791$ GHz and the sky location of GN-z11. The upper limits show that GN-z11 is neither luminous in $L_{\rm IR}$ nor $L_{\rm [C\,II]}$, with a dust mass 3 σ limit of log ($M_{\rm dust}/{\rm M}_\odot$) < 6.5 − 6.9 and with a [C II] based molecular gas mass 3 σ limit of log ($M_{\rm mol,\,[C\,II]}/{\rm M}_\odot$) < 9.3. Together with radiative transfer calculations, we also investigated the possible cause of the dust poor nature of the GN-z11 showed by the blue colour in the UV continuum of GN-z11 ($\beta_{\rm UV} = -2.4$), and found that $\gtrsim$3 × deeper observations are crucial to study dust production at very high-redshift. Nevertheless, our observations show the crucial role of deep mm/submm observations of very high-redshift galaxies to constrain multiple phases in the interstellar medium.

Key words: (ISM:) dust, extinction – galaxies: formation – galaxies: ISM.

1 INTRODUCTION

The first few hundred million years after the big bang at redshifts of $z > 10$ are the last major unexplored epoch in the history of the Universe. Recently, the arrival of the *JWST* has opened a completely new window to observe the very high redshift Universe. *JWST*/NIRCam's unprecedented sensitivity at infrared wavelengths has enabled confident photometric information on $z_{\rm phot} > 10$ candidates detected over multiple bands (e.g. Castellano et al. 2022; Finkelstein et al. 2022; Naidu et al. 2022; Hainline et al. 2023; Harikane et al. 2023). At the same time, spectroscopy with *JWST*

★ E-mail: yoshinobu.fudamoto@gmail.com

obtained multiple emission lines in the rest-frame UV to optical wavelength, providing unambiguous spectroscopic redshifts (e.g. Morishita et al. 2022; Roberts-Borsani et al. 2022; Boyett et al. 2023; Cameron et al. 2023; Matthee et al. 2023; Williams et al. 2023; Bunker et al. 2023b) and unprecedented diagnostic power of interstellar medium (ISM) properties for the first time (e.g. Tacchella et al. 2022; Carnall et al. 2023; Laseter et al. 2023; Nakajima et al. 2023; Sanders et al. 2023). This started to reveal a detailed picture of galaxy formation at $z > 10$, which was extremely challenging to reach before the *JWST* era (see Madau & Dickinson 2014, for a review).

GN-z11 is the highest redshift galaxy identified using the *Hubble Space Telescope (HST)* and the *Spitzer Space Telescope* (Oesch et al. 2016). GN-z11 was first identified from *HST* imaging data from the Cosmic Assembly Near-infrared Deep Extragalactic Legacy Survey (CANDELS: Bouwens et al. 2010; Grogin et al. 2011; Koekemoer et al. 2011). In particular, it lies in the deepest area of CANDELS in the north Great Observatories Origins Deep Survey (GOODS) field at RA, Dec. = 12:36:25.46, +62:14:31.4 (J2000).GN-z11 was found to be the brightest galaxy candidate at $z > 10$ (Bouwens et al. 2015; Oesch et al. 2015). From *HST* WFC3/IR G141 slitless grism spectroscopy, the galaxy had a redshift of $z_{\rm grism} = 11.09^{+0.08}_{-0.12}$ through the identification of the Ly α continuum break (Oesch et al. 2016).

Due to the extremely high ultraviolet (UV) luminosity of $M_{\rm UV} = -21.6$, detailed *JWST* observations of GN-z11 have already been performed. The *JWST* Advanced Deep Extragalactic Survey (JADES; Eisenstein et al. 2023) obtained deep *JWST* NIRSpec slit spectroscopy and confirmed its redshift to be $z = 10.6034 \pm 0.0013$ based on detections of multiple emission lines (Bunker et al. 2023a). Together with photometric information obtained with *JWST* NIRCam imaging, studies confirmed that GN-z11 is the most UV luminous galaxy at $z > 10$ known to date (e.g. Hainline et al. 2023; Harikane et al. 2023). In particular, the extremely compact morphology ($R_{\rm e} = 64 \pm 20$ pc; Tacchella et al. 2023) and the large UV luminosity ($M_{\rm UV} = -21.6 \pm 0.02$; Tacchella et al. 2023) suggest that GN-z11 could represent very early onset of active galactic nucleus (AGN) activity (Maiolino et al. 2023a) or that it shows possible signatures of Population III stars in its surrounding blob (Maiolino et al. 2023b). At the same time, the significant detection of nitrogen emission lines (N IV] 1486 Å and N III] 1750 Å) and the large overabundance seen in the N/O ratio could require a new scenario of nitrogen production and/or oxygen depletion (Cameron et al. 2023), such as the formation of supermassive stars through stellar collisions in an extremely dense environment (Charbonnel et al. 2023).

With the newly obtained detailed observations from *JWST*/NIRCam and *JWST*/NIRSpec, GN-z11 remains one of the most important galaxies at $z > 10$ to understand gas fuelling mechanism for galaxy growths and dust production in the early Universe. To fully understand the formation of this remarkably luminous galaxy and to constrain the formation mechanisms of massive galaxies at $z > 10$, it is essential to investigate multiple components of its interstellar medium (ISM) as well as dust formation and dust-obscured star formation activity. In addition to the rest-frame UV images and spectra, information about the dust and neutral ISM properties from rest-frame far-infrared (FIR) spectroscopy is thus required to provide a comprehensive picture arising from observations covering a wide wavelength range (see Carilli & Walter 2013; Hodge & da Cunha 2020, for reviews).

Here, we report millimetre wavelength observations of GN-z11 using the Northern Extended Millimeter Array (NOEMA), targeting the dust continuum and the [C II] 158 μm emission line. Using the highly sensitive data obtained for GN-z11, we constrain its ISM properties, dust-obscuration, as well as dust production efficiency by comparing with dust enrichment and geometry models from Ferrara et al. (2022).

This paper is organized as follows: in Section 2, we summarize the NOEMA observations so far performed for GN-z11. In Section 3, we present our data analysis and measurements for the [C II] 158 μm emission line and $\lambda \sim 160\,\mu$m dust continuum. In Section 4, we present the results. We present discussions in Section 5. Finally, we conclude with the summary in Section 6. Throughout this paper, we assume a cosmology with $(\Omega_m, \Omega_\Lambda, h) = (0.3, 0.7, 0.7)$, and the Chabrier (Chabrier 2003) initial mass function (IMF), where applicable. With these cosmological parameters, 1 arcsec corresponds to 4.0 kpc in proper coordinate and the luminosity distance is 1.11×10^5 Mpc at $z = 10.603$.

2 OBSERVATIONS

2.1 NOEMA observations

Over the past years, NOEMA has targeted GN-z11 to search for the [C II] 158 μm emission line based on the redshift estimated from its early photometric and grism data from *HST* to explore its emission in the FIR. Deep NOEMA observations were conducted as separate observation projects across four cycles in the years 2014, 2016, 2018, and 2019. We summarize these observations in the following:

Observations in 2014: Using the WideX correlator, GN-z11 was observed by scanning the frequency range between 161.9 and 176.3 GHz (PI: C. Carilli). With six antennae, four different frequency settings were used. Each tuning has a 3.6 GHz bandwidth. The total on-source time was 46.6 h, most of the data were taken in good to excellent conditions, and little flagging was required. The spectral scan observations aimed to search for [C II] 158 μm emission line covering redshifts of $z \sim 9.78 - 10.74$, i.e. a photometric redshift range estimated based on the *HST* and *Spitzer* photometry (Bouwens et al. 2015; Oesch et al. 2015).

Observations in 2016: Using a single tuning with the WideX correlator, GN-z11 was observed with eight antennae (PI: F. Walter and P. Oesch). The on-source time was 5.2 h in good weather conditions. Data calibration was done in a standard manner at IRAM, and only minor flagging was required. The frequency between 155.2 and 158.8 GHz was tuned to target [C II] emission line at redshifts between 10.97 and 11.25 based on the updated redshift estimation using the *HST* grism spectroscopy (Oesch et al. 2016).

Observations in 2018: Deeper spectral scans were performed for GN-z11 with nine antennae and with the newly installed Polyfix correlator in 2018 (PI: F. Walter and P. Oesch). With a total on-source time of 17.4 h, two Polyfix tunings were used to cover the frequency range between 152.9 and 163.6 GHz. These observations aimed to observe [C II] within the redshift range of $z_{\rm [C\,II]} = 10.62 - 11.43$. Compared to the 2016 observations, these observations were deeper and covered a wider frequency range. The weather conditions were good. Data calibration was performed in a standard manner at IRAM, and minor flagging was required.

Observations in 2019: Follow-up observations of GN-z11 were again performed with 10 antennae with the Polyfix correlator (PI: F. Walter and P. Oesch). Total on-source time was 11.4 h. A single tuning of the Polyfix correlator covered 156.9 − 164.6 GHz, covering [C II] redshifts between $z_{\rm [C\,II]} = 10.55 - 11.11$. Weather conditions were generally good and minor flagging was required. We note that the observations in 2019 eventually covered the [C II] emission line from the actual spectroscopic redshift ($z_{\rm spec} = 10.60$; Bunker et al. 2023a) of GN-z11 using the updated NOEMA interferometer.

All the calibrations of phase, absolute flux, and amplitude were performed using the GILDAS software[1] with the support of IRAM astronomers.

2.2 JWST observations

We obtained near-IR (NIR) images of GN-z11 from a *JWST* cycle-1 medium programme entitled 'First Reionization Epoch Spectroscopic Complete Observation' (FRESCO; Oesch et al. 2023). We used the *F444W* image as a sky location prior for extracting a spectrum and searching for dust continuum emission associated with GN-z11. A comprehensive description of the survey design, data reduction, and analysis can be found in Oesch et al. (2023).

Using *JWST* NIRCam (Rieke, Kelly & Horner 2005), FRESCO performed deep slitless grism observations in the northern and southern GOODS/CANDELS fields using *F444W* filters with a medium spectral resolution of $R = 1600$. Simultaneously, broad- and medium-band images of the fields were acquired using the *F444W*, *F210M*, and *F182M* bands. The imaging integration times were 0.26, 1, and 1.2 h per pointing for *F444W*, *F210M*, and *F182M* bands, respectively. The data were reduced using the GRIZLI software (v1.7.11), which is publicly available (Brammer 2018; Brammer et al. 2022). The $5\,\sigma$ depth of the observations for the *F444W* imaging is ~ 28.2 mag for imaging observations (Oesch et al. 2023).

3 ANALYSIS

3.1 Dust continuum, IR luminosity, and dust mass

Using the GILDAS package CLIC, the combined continuum UV table of GN-z11 was made using all existing NOEMA data. We then imaged the continuum data using the GILDAS MAPPING package using a pixel size of 0.4 arcsec. The resulting continuum map has a synthesized beam full width at half-maximum (FWHM) of 2.05 arcsec × 1.83 arcsec, and an RMS of 13 μJy beam^{-1}. In the continuum image, we only find a $\sim 2\,\sigma$ signal ~1 arcsec offset from GN-z11, and found no clear signals co-located with the *JWST* NIRCam *F444W* detection of GN-z11 (Fig. 1). Thus, we concluded that the dust continuum of GN-z11 is not detected from the existing NOEMA observations.

As the dust continuum is not detected, we estimated upper limits for the dust continuum emission and IR luminosity. Using the RMS of the continuum image, we obtained a $3\,\sigma$ upper limit of $< 39\,\mu$Jy. The upper limit of IR luminosity is then estimated by assuming an FIR spectral energy distribution (SED) for the GN-z11 by integrating a modified blackbody function between the rest-frame wavelength of $8 - 1000\,\mu$m. In particular, we assumed a dust temperature of $T_{\rm d} = 82$ K by extrapolating a dust temperature evolution estimated in Sommovigo et al. (2022).[2] The derived dust temperature of 82 K is much higher (by $\gtrsim 30$ K) than those of $z \sim 7$ galaxies (e.g. Algera et al. 2024) but consistent with that currently estimated from one of the highest redshift dust detection at $z = 8.31$ (> 80 K; Bakx et al. 2020). We discuss impacts of assuming a lower dust temperature in Section 3.1.1. We also assumed a dust emissivity index of $\beta = 2.0$ as is also assumed when estimating $T_{\rm d}$ in Sommovigo et al. (2022), and applied a correction of the cosmic microwave background (CMB) attenuation based on da Cunha et al. (2013). Due to the high CMB temperature of 31.7 K at $z = 10.603$, the CMB attenuation with the assumed dust temperature is large and we need to multiply the dust continuum emission by 1/0.88. Finally, we obtained a $3\,\sigma$ upper limit for the IR luminosity of $< 3.6 \times 10^{12}\,{\rm L}_{\odot}$.

Using the $3\,\sigma$ continuum upper limit and the assumed dust temperature of $T_{\rm d} = 82$ K, we estimated a dust mass upper limit in GN-z11. We used a dust mass absorption coefficient of $\kappa_{\rm d}(\lambda_{\rm rest}) = 30 \times (100\,\mu{\rm m}/\lambda_{\rm rest})^{\beta}\,{\rm cm}^2\,{\rm g}^{-1}$ (Inoue et al. 2020), which is estimated as a typical value from different dust compositions and temperatures using laboratory experiments (e.g. Mennella et al. 1998; Chihara, Koike & Tsuchiyama 2001; Boudet et al. 2005). We then applied a correction for the CMB and obtained a dust mass upper limit of $\log{(M_{\rm d}/{\rm M}_{\odot})} < 6.5\,(3\,\sigma)$.

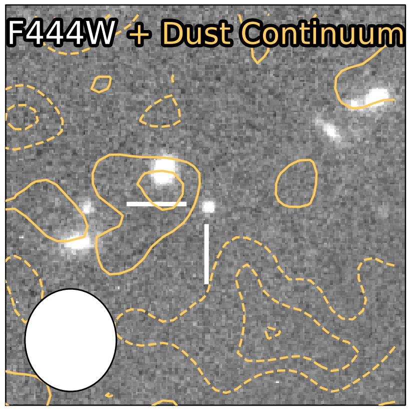

Figure 1. 8 arcsec × 8 arcsec cutout of the *JWST F444W* image obtained by the FRESCO *JWST* survey (background; Oesch et al. 2023) and dust continuum (contours) of GN-z11: solid contours show 1σ and $2\,\sigma$ and dashed contours show -3σ, -2σ, -1σ where $1\,\sigma = 13.0\,\mu$Jy beam^{-1}. The filled ellipse in the lower left corner shows the synthesized beam FWHM of the combined dust continuum image (2.1 arcsec × 1.8 arcsec).

3.1.1 Dust temperature uncertainty

The typical dust temperature of star-forming galaxies at very high redshift is unconstrained from observations. Moreover, the assumed dust temperature has a large impact on the estimated IR luminosity (see discussion e.g. by Ferrara et al. 2017; Ma et al. 2019; Faisst et al. 2020; Fudamoto et al. 2020; Lower et al. 2023). Especially, our assumed dust temperature is much higher than those directly measured in lower redshift galaxies (e.g. $T_{\rm d} \sim 45$ K at $z \sim 5 - 7$; Liang et al. 2019; Béthermin et al. 2020; Faisst et al. 2020; Algera et al. 2023). Thus, to test the assumed dust temperature and to understand its impact on the IR luminosity upper limit, we employed an alternative method to estimate a dust temperature limit.

We tested the assumed dust temperature using the FIS22 code presented in Fudamoto, Inoue & Sugahara (2022). FIS22 uses simple assumptions about star-to-ISM geometry and the radiation equilibrium between dust attenuation and re-emission. Using the measured size of the star-forming region, the code allows us to obtain estimations of dust temperature from a single FIR continuum observation. To estimate the limit, we assumed the size of the star-forming region from the UV emission (i.e. $R_{\rm e} = 64 \pm 20$ kpc; Tacchella et al. 2023), and the average ISM clumpiness parameter of $\log \xi_{\rm clp} = -1.02$ as found in Fudamoto et al. (2022). With a fixed size and an upper limit on FIR emission, we are able to obtain a lower limit on dust temperature. With the assumed dust size and UV luminosity of $L_{\rm UV} = 7.40 \pm 0.01 \times 10^{11}\,{\rm L}_{\odot}$, we obtained

[1] https://www.iram.fr/IRAMFR/GILDAS/

[2] We assumed transmissivity of the ISM to be $T = 0.9$ as assumed by Fujimoto et al. (2022), and a gas phase metallicity of 0.04 $Z_{\odot}$ obtained in the SED fitting in Tacchella et al. (2023).

Table 1. Measured properties of GN-z11 from NOEMA observations.

NOEMA measurements	
$f_{[\mathrm{C\,II}]}$	$<29\,\mathrm{mJy\,km\,s^{-1}}$ ($3\,\sigma$ limit)
log ($L_{[\mathrm{C\,II}]}/L_{\odot}$)	<8.2 ($3\,\sigma$ limit)
$f_{\mathrm{cont},160\,\mu\mathrm{m}}$	$<39\,\mu$Jy ($3\,\sigma$ limit)
log (L_{IR} / $L_{\odot}$)	<12.5 (with $T_{\mathrm{d}}=82$ K)
	<11.9 (with $T_{\mathrm{d}}=54$ K)
log (M_{d} / $M_{\odot}$)	<6.5 (with $T_{\mathrm{d}}=82$ K)
	<6.9 (with $T_{\mathrm{d}}=54$ K)
	and $\kappa_d(\lambda_{\mathrm{rest}})=30\times(100\,\mu\mathrm{m}/\lambda_{\mathrm{rest}})^{\beta}\,\mathrm{cm^2\,g^{-1}}$)

$T_{\mathrm{d}} > 54$ K. The derived lower limit indeed supports the high dust temperature of T_{d} assumed in our calculation. We note that the estimated dust temperature and its limit is still uncertain as the method assumes that the dust has the same spatial distribution as the UV emission. Nevertheless, we use the $T_{\mathrm{d}}=54$ K as a lower limit case as it currently gives the lowest T_{d} estimation.

In this lower limiting dust temperature case of $T_{\mathrm{d}}=54$ K, we find the $3\,\sigma$ upper limit of IR luminosity to be $<7.7\times10^{11}\,L_{\odot}$ (i.e. $\sim\times5$ smaller than that found by assuming $T_{\mathrm{d}}=82$ K). We further noticed that a dust temperature assumption lower than 50 K does not change the IR luminosity upper limit as the CMB correction becomes large and mitigates the difference of the dust temperature assumption. Thus, a systemic uncertainty of a factor $\sim$5 is very conservative. In the following discussions, we derive several estimates based on assuming the 82 and 54 K dust temperatures.

All the estimated quantities are summarized in Table 1.

3.2 [C II] 158 μm emission line

The sky frequency of the [C II] 158 μm emission line of GN-z11, $\nu_{[\mathrm{C\,II}]-\mathrm{sky}}=163.791$ GHz, is covered by the observations in 2014 and 2019. From these observations, we focus on the observations of 2019 in our analysis which has much higher sensitivity than that of 2014 by using upgraded receivers with 10 antennae. Using the GILDAS MAPPING package, we created a data cube with 50 km s^{-1} spectral binning with a pixel angular size of 0.4 arcsec. The resulting data cube has an RMS of ~0.31 mJy beam^{-1} in the 50 km s^{-1} binning at $\nu=163.791$ GHz.

We then extracted a spectrum of GN-z11 using a circular aperture with a radius of $r=1$ arcsec on top of the *JWST* detection of GN-z11 (left panel of Fig. 2). The 1 arcsec radius is consistent with the NOEMA beam size. At the frequency of [C II] at $z=10.603$, we only find $<1\,\sigma$ signals in the spectra. To search for any spatially off-set signals, we further created a [C II] 158 μm emission moment-0 map. To create the [C II] moment-0 image, we assumed the line width of [C II] emission to be 150 km s^{-1}, which is consistent with recent FIR emission line observations of $z>9$ galaxies (e.g. Hashimoto et al. 2018). In the surrounding area of the GN-z11, we only find $\sim1\,\sigma$ signals (Fig. 2) which is much lower than the typical secure detection thresholds for lines with well-known sky location and spectroscopic redshift (e.g. $>3.5\,\sigma$; Béthermin et al. 2020). Based on these results, we concluded that the [C II] 158 μm emission line is not detected in the current NOEMA data.

Based on the non-detection, we measured a $3\,\sigma$ upper limit of the [C II] emission line luminosity by measuring three times the pixel-by-pixel RMS of the moment-0 map. We obtained a $3\,\sigma$ [C II] flux upper limit of 0.087 Jy km s^{-1}, and $L_{[\mathrm{C\,II}]}$ upper limit of GN-z11 of $<1.7\times10^{8}\,L_{\odot}$.

All the estimated quantities are summarized in Table 1.

4 RESULTS

4.1 Dust obscured star formation activity of GN-z11

With the relatively high upper limit of L_{IR}, the dust-obscured star formation rate (SFR) is only weakly constrained with $\mathrm{SFR_{IR}}<430\,\mathrm{M_{\odot}\,yr^{-1}}$ with $T_{\mathrm{d}}=82$ K and $<92\,\mathrm{M_{\odot}\,yr^{-1}}$ with $T_{\mathrm{d}}=54$ K assuming a conversion of $\mathrm{SFR_{IR}}=1.2\times10^{-10}\,L_{\mathrm{IR}}\,\mathrm{M_{\odot}\,yr^{-1}\,L_{\odot}^{-1}}$ (Madau & Dickinson 2014; Inami et al. 2022). The weak upper limit on $\mathrm{SFR_{IR}}$ despite the deep continuum observations is due to the assumed high dust temperature of $T_{\mathrm{d}}=82$ and 54 K. Using these limits, the infrared excess (IRX = log ($L_{\mathrm{UV}}/L_{\mathrm{IR}}$); Meurer, Heckman & Calzetti 1999) $3\,\sigma$ limit of GN-z11 is estimated to be >-0.9 to >-1.5. To further constrain the dust obscured star formation activity of GN-z11, accurate constraints on the dust temperature is essential via deep observations at wavelengths <1 mm.

With the estimated stellar mass of $\sim10^{9}\,\mathrm{M_{\odot}}$ (Tacchella et al. 2023), the dust mass upper limit shows a stellar-to-dust mass ratio of $\xi_{\mathrm{d}}\lesssim0.003$ for $T_{\mathrm{d}}=82$ K and $\xi_{\mathrm{d}}\lesssim0.008$ for $T_{\mathrm{d}}=54$ K. These limits are consistent with typical values in lower redshift galaxies (e.g. Calura et al. 2017; Dayal et al. 2022).

4.2 [C II] 158 μm emission line

To compare the star formation activity and $L_{[\mathrm{C\,II}]}$ of GN-z11, we adopted the total SFR of $21^{+22}_{-10}\,\mathrm{M_{\odot}\,yr^{-1}}$ obtained in the SED fitting in Tacchella et al. (2023). We find that based on the upper limit $L_{[\mathrm{C\,II}]}$ from our measurement, GN-z11 has $L_{[\mathrm{C\,II}]}$ consistent with or slightly smaller than that of low redshift similarly star-forming galaxies (Fig. 3). Although few observational studies of the SFR-$L_{[\mathrm{C\,II}]}$ relation for galaxies at $z>10$, this shows that the [C II] luminosity of GN-z11 is not enhanced compared with the relation obtained for star-forming galaxies at lower redshifts.

The existence of an AGN was proposed in GN-z11 based on the significant detection of [Ne IV] λ2423 using deep NIRSpec observation (Maiolino et al. 2023a). If the rest-frame UV emission of GN-z11 is dominated by AGN activity, the SFR of GN-z11 might be overestimated and thus our constraints on the SFR-$L_{[\mathrm{C\,II}]}$ relation of GN-z11 should be lifted. Further, to conclusively compare with metallicity dependent [C II] – SFR scaling relations (e.g. Vallini et al. 2015), deeper [C II] observations are required.

5 DISCUSSION

5.1 Molecular gas mass and gas depletion time-scale at $z=10.6$

Recent studies showed that the dominant fraction of [C II] 158 μm emission lines arise from neutral gas, such as neutral photo-dissociation regions (PDRs). In particular, luminous galaxies typically have >80 per cent of the [C II] emission originate from the PDRs (Díaz-Santos et al. 2017). For high-redshift galaxies, this feature is further supported by detailed calculations and observations of emission lines arising from H II regions (Decarli et al. 2014, 2022; Witstok et al. 2022). This makes the [C II] 158 μm emission line an excellent tracer of star-forming neutral gas (e.g. Zanella et al. 2018; Sommovigo et al. 2021, see also Madden et al. 2020 for metallicity dependence of the [C II] to the molecular gas mas conversion factor).

Using the formalism presented in Zanella et al. (2018), we estimate the upper limit of the molecular gas mass of GN-z11 to be log ($M_{\mathrm{mol}}/\mathrm{M_{\odot}}$) <9.7. With the estimated stellar mass of $\sim10^{9}\,\mathrm{M_{\odot}}$ (Tacchella et al. 2023), the molecular gas fraction ($f_{\mathrm{mol}}=M_{\mathrm{mol}}/(M_{\mathrm{star}}+M_{\mathrm{mol}})$) of GN-z11 is $f_{\mathrm{mol}}<0.83$ ($3\,\sigma$). The upper limit from the

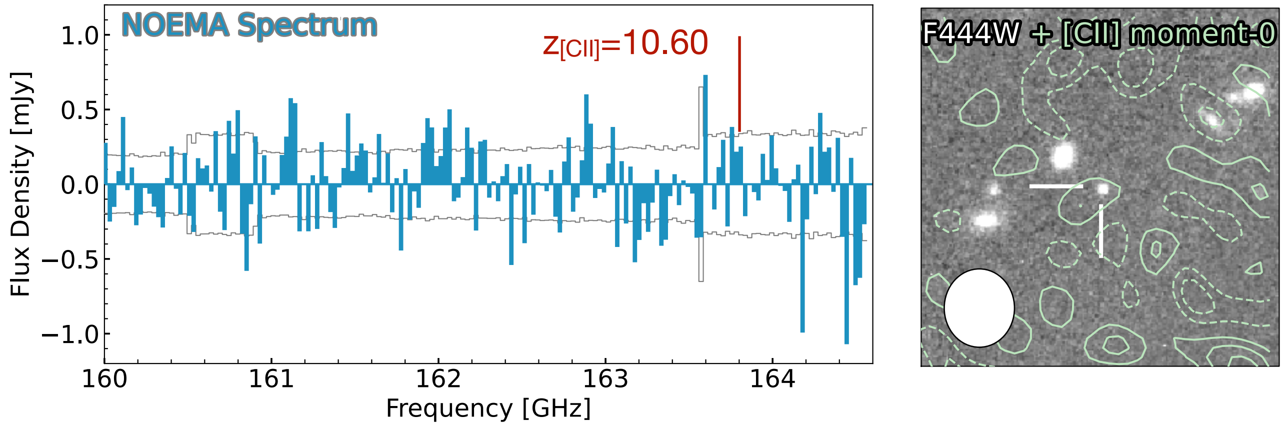

Figure 2. *Left panel*: The NOEMA spectrum of GN-z11 with 50 km s^{-1} binning. The solid lines across the entire frequency range show the RMS of each channel. The NOEMA observation covers [C II] 158 μm emission line of GN-z11 at the observed frequency of $\nu_{\rm obs} = 163.84$ GHz with the $z_{\rm spec} = 10.60$ (vertical line). From the data cube and extracted spectrum, we do not find any signal of the [C II] emission line. *Right panel*: 8 arcsec × 8 arcsec cut-out of *JWST F444W* image (background) and [C II] emission line moment-0 map (contours) of GN-z11. Contours show 1σ, 2σ, and 3σ and dashed contours show -3σ, -2σ, and -1σ. The moment-0 map of the data cube is made by integrating over the 150 km s^{-1} of the [C II] emission line frequency. RMS of the image is 29 mJy km s^{-1}, providing a 3 σ upper limit of [C II] luminosity < 1.7 × 10^8 L$_\odot$.

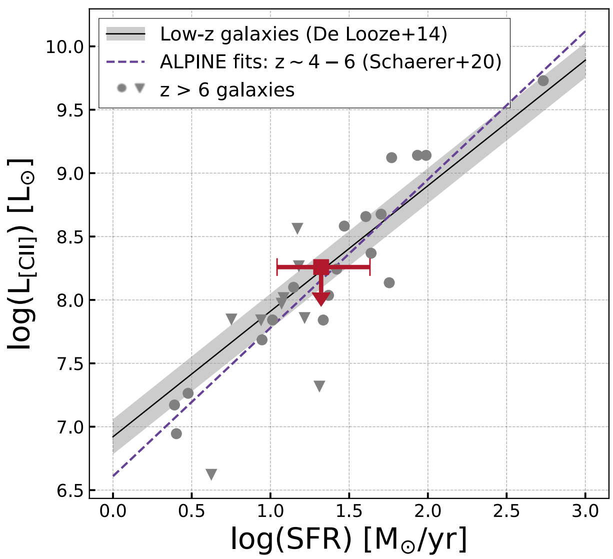

Figure 3. SFR versus [C II] emission line luminosity of GN-z11. Previous observations of $z > 6$ are also plotted with grey points (Harikane et al. 2020; Schouws et al. 2023; Fudamoto et al. 2023 and references therein). Downward triangles show 3 σ upper limit in case of non-detections. Lines show previously obtained relations for low- and high-redshift galaxies (solid: Schaerer et al. 2020, dashed: De Looze et al. 2014). For the SFR of GN-z11, we adopted the SED fitting results of 21^{+22}_{-10} M$_\odot$ yr^{-1} from Tacchella et al. (2023).

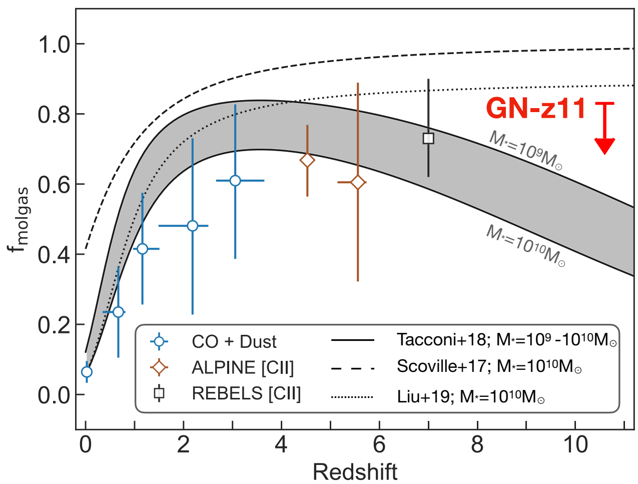

Figure 4. Evolution of the molecular mass fraction ($f_{\rm molgas} = M_{\rm molgas}/(M_{\rm molgas} + M_{\rm star0})$) across a wide redshift range. Various indicators are used to estimate molecular gas mass: CO emission lines and dust continuum at $z < 4$ (Dessauges-Zavadsky et al. 2017; Scoville et al. 2017; Tacconi et al. 2018; Tacconi, Genzel & Sternberg 2020, see also Boogaard et al. 2020), [C II] emission lines at $4 < z < 6$ from the ALMA Large Program to Investigate C+ at Early Times survey (ALPINE; Dessauges-Zavadsky et al. 2020), and at $z \sim 7$ from the Reionization Era Bright Emission Line Survey (REBELS; Aravena et al. 2024).Data points for the $z < 8$ samples represent mean values and errorbars are 16th to 84th percentiles within the distribution. Upper limit of GN-z11 is within the range of $z > 4$ galaxy observations.

[C II] observations is largely consistent with lower redshift galaxies (Fig. 4).

We checked the estimation with the Kennicutt–Schmidt law (e.g. Kennicutt & Evans 2012). Although it is unknown if the Kennicutt–Schmidt law found in lower redshift Universe is applicable to high-redshift galaxies, we found total gas mass of log (M$_{\rm gas}$/M$_\odot$) = 8.8 by using the relation found in Daddi et al. (2010) and the SFR of 21 M$_\odot$ yr^{-1} (Tacchella et al. 2023). We found the estimated value is consistent with the upper limit derived from the upper limit of [C II] luminosity, although the derived value could be largely uncertain due to the uncertainty of the Kennicutt–Schmidt law in the very high redshift Universe.

With the estimated SFR of 21 M$_\odot$ yr^{-1} (Tacchella et al. 2023) and the molecular gas upper limit of log (M$_{\rm mol}$/M$_\odot$) < 9.7 from the [C II] observation, the upper limit of the molecular gas depletion time of GN-z11 is $t_{\rm depl}$ < 0.2 Gyr (3 σ). There are two possible uncertainties for the estimated gas depletion time. One is an uncertainty of the contribution from the AGN to the UV luminosity, which could make the SFR estimation uncertain. Another is the possible high neutral atomic-to-molecular gas fraction in the ISM. Simulations, indeed, suggest significant fractions of neutral gas exist as an atomic phase in low mass galaxies, although the estimations are uncertain due to systemic uncertainties (e.g. Diemer et al. 2018). While these possible uncertainties could exist, the currently estimated molecular gas mass and the SFR suggests that GN-z11 might deplete all molecular gases before $z \gtrsim 8$, unless molecular gas is rapidly replenished by accretion.

Recent CO and [CI] emission line observations using $z \sim 6$ AGNs suggest that [C II] based molecular gas mass measurements could be systematically higher by ~ 0.5 dex compared with those estimated from [C I] and/or CO observations (Neeleman et al. 2021; Decarli et al. 2022). Thus if the ~ 0.5 dex overprediction is the case for our estimations, the upper limit might need to be systematically lowered, providing stronger constraints. Deeper observations of the [C II] emission line and observations of other molecular gas indicator (e.g. emission lines from [C I] and/or CO) will be crucial to further constrain these essential parameters of galaxy growth.

5.2 Expected dust opacity and constraints on the dust formation

Here, we compare our dust continuum upper limits with recent theoretical analysis of $z > 10$ UV luminous galaxies (e.g. Ferrara, Pallottini & Dayal 2023).

Ferrara et al. (2023) discussed that the *JWST* based finding of very blue and compact galaxies was surprising. Indeed, the observed dust optical depth at the rest-frame 1500 Å deduced for GN-z11 is $\tau_{1500} = 0.49$ (corresponding to $A_V = 0.17$, Bunker et al. 2023b). This low value does not agree with the expected dust optical depth estimated from the extremely compact effective radius ($r_e = 64$ pc; Tacchella et al. 2023) and the dust mass associated with the estimated massive stellar mass ($\sim 10^9\,M_\odot$). By assuming a standard dust-to-stellar mass ratio $\xi_d \sim 0.002$, appropriate for a Salpeter IMF ($1 - 100\,M_\odot$) and a dust yield of 0.1 $M_\odot$ per supernova, we estimate a dust mass of $M_d \sim 10^6\,M_\odot$ (e.g. Hirashita et al. 2014). This simple estimate of dust mass is consistent with the estimated age of GN-z11 (18 Myr; Bunker et al. 2023a) and recent stellar evolution tracks (e.g. Schaerer et al. 2022). If UV and dust are co-located in the tiny ~ 64 pc region, using the calculation performed in Ferrara et al. (2023), we estimated that the resulting optical depth would be $\tau_{1500} \sim 500$, i.e. far exceeding the observed value.

The dust envelope can be made less opaque if the dust has a spatial distribution that is much more extended than the stellar r_e. In particular, assuming a spherical dust distribution, the observed value $\tau_{1500} = 0.49$ is recovered if the dust distribution is expanded out to $r \sim 30 \times r_e$ to $100 \times r_e$ (i.e. ~ 2 to ~ 6.4 kpc). Physically, this configuration can be achieved, for example as a result of an outflow emanating from the galaxy. The presence of radiation-driven dusty outflows could arise from the super-Eddington nature of galaxies like GN-z11 (Ferrara et al. 2023; Fiore et al. 2023; Ziparo et al. 2023).

In our observations, we find a $\lambda_{rest} = 160\,\mu$m dust continuum of $< 13\,\mu$Jy at $1\,\sigma$ ($< 26\,\mu$Jy, $2\,\sigma$). This value is higher than the predicted one at any stage during the outflow expansion. In fact, when the outflow has expanded the dust distribution so as to produce the observed value of τ_{1500}, we predict that the 160 μm flux should be 4.5 μJy, hence about 3 times below our upper limit. Clearly, uncertainties are related to the assumed value of ξ_d. The present observations, however, can be used to obtain a limit on $\xi_d < 0.014$ at $1\,\sigma$ ($\xi_d < 0.32$ at $2\,\sigma$), which translates a predicted upper limit on the dust mass of $< 7 \times 10^6\,M_\odot$ ($< 1.6 \times 10^8\,M_\odot$). Thus, at least $3 \times$ deeper continuum observations would be crucial to provide constraints on dust formation at $z > 10$ and to test the proposed scenario to explain the very blue colour of high-redshift massive compact galaxies.

6 CONCLUSION

In this paper, we present results based on NOEMA observations of GN-z11 targeting the [C II] 158 μm emission line and the underlying dust continuum from a UV luminous star-forming galaxy GN-z11 at $z = 10.60$. We found the following results:

(i) Although NOEMA observations were extremely deep and covered the sky frequency of the [C II] 158 μm emission line, we did not detect either [C II] 158 μm or dust continuum. We reported $3\,\sigma$ upper limits of the [C II] luminosity ($L_{[C\,II]} < 1.7 \times 10^8\,L_\odot$) and the IR luminosity ($L_{IR} < 3.6 \times 10^{12}\,L_\odot$).

(ii) Based on the upper limits, we found that GN-z11 is not bright either in [C II] emission or dust continuum. The upper limit $L_{[C\,II]}$ of GN-z11 is consistent or could be slightly smaller than that predicted from the SFR-$L_{[C\,II]}$ relation observed from lower redshift galaxies at $z < 8$.

(iii) As [C II] emission mostly traces the neutral ISM, we estimate a molecular gas mass for GN-z11 using the relation in Zanella et al. (2018). We find an upper limit of $M_{mol} < 5.0 \times 10^9\,M_\odot$, and a depletion time of < 0.2 Gyr, suggesting that the GN-z11 could deplete all the star-forming gas by $z \gtrsim 8$.

(iv) The blue colour ($\beta = -2.4$) suggests that GN-z11 is dust poor, which is consistent with the non-detection of dust continuum. The current upper limit is $> \times 2$ above the expected continuum flux density expected assuming typical dust production.

Our observations of GN-z11 showcase the crucial constraints that submm/mm observations can provide for very early galaxies.

ACKNOWLEDGEMENTS

This work is based on observations carried out under project numbers XACE, XBCE, XCCE, XDCE, S16CQ, W17FD, and W18FD with the IRAM NOEMA Interferometer. IRAM was supported by INSU,CNRS (France), MPG (Germany), and IGN (Spain). YF, AKI, and YS acknowledge support from National Astronomical Observatory of Japan (NAOJ) ALMA Scientific Research grant number 2020-16B. YF further acknowledges support from JSPS KAKENHI grant numbers JP22K21349 and JP23K13149. PAO acknowledges support from the Swiss National Science Foundation through project grant number 200020_207349. The Cosmic Dawn Center (DAWN) is funded by the Danish National Research Foundation under grant number 140. HD acknowledges financial support from the Agencia Estatal de Investigación del Ministerio de Ciencia e Innovación (AEI–MCINN) under grant (La evolución de los címulos de galaxias desde el amanecer hasta el mediodía cósmico) with reference (PID2019-105776GB-I00/DOI:10.13039/501100011033).

DATA AVAILABILITY

The data underlying this article will be shared on reasonable request to the corresponding author.

REFERENCES

Algera H. et al., 2024, MNRAS, 527, 6867
Bakx T. J. L. C. et al., 2020, MNRAS, 493, 4294
Béthermin M. et al., 2020, A&A, 643, A2
Boogaard L. A. et al., 2020, ApJ, 902, 109

Boudet N., Mutschke H., Nayral C., Jäger C., Bernard J. P., Henning T., Meny C., 2005, ApJ, 633, 272
Bouwens R. J. et al., 2010, ApJ, 725, 1587
Bouwens R. J., Illingworth G. D., Oesch P. A., Caruana J., Holwerda B., Smit R., Wilkins S., 2015, ApJ, 811, 140
Boyett K. et al., 2023, preprint (arXiv:2303.00306)
Brammer G., 2018, Gbrammer/Grizli: Preliminary Release. Zenodo. Available at: https://doi.org/10.5281/zenodo.1146905
Brammer G., Strait V., Matharu J., Momcheva I., 2022, grizli, Zenodo. Available at: https://doi.org/10.5281/zenodo.6672538
Bunker A. J. et al., 2023a, A&A, 677, A88
Bunker A. J. et al., 2023b, preprint (arXiv:2306.02467)
Calura F. et al., 2017, MNRAS, 465, 54
Cameron A. J., Katz H., Rey M. P., Saxena A., 2023, MNRAS, 523, 3516
Carilli C. L., Walter F., 2013, ARA&A, 51, 105
Carnall A. C. et al., 2023, MNRAS, 518, L45
Castellano M. et al., 2022, ApJ, 938, L15
Chabrier G., 2003, PASP, 115, 763
Charbonnel C., Schaerer D., Prantzos N., Ramírez-Galeano L., Fragos T., Kuruvandothi A., Marques-Chaves R., Gieles M., 2023, A&A, 673, L7
Chihara H., Koike C., Tsuchiyama A., 2001, PASJ, 53, 243
da Cunha E. et al., 2013, ApJ, 766, 13
Daddi E. et al., 2010, ApJ, 714, L118
Dayal P. et al., 2022, MNRAS, 512, 989
De Looze I. et al., 2014, A&A, 568, A62
Decarli R. et al., 2014, ApJ, 782, L17
Decarli R. et al., 2022, A&A, 662, A60
Dessauges-Zavadsky M. et al., 2017, A&A, 605, A81
Dessauges-Zavadsky M. et al., 2020, A&A, 643, A5
Díaz-Santos T. et al., 2017, ApJ, 846, 32
Diemer B. et al., 2018, ApJS, 238, 33
Eisenstein D. J. et al., 2023, preprint (arXiv:2306.02465)
Faisst A. L., Fudamoto Y., Oesch P. A., Scoville N., Riechers D. A., Pavesi R., Capak P., 2020, MNRAS, 498, 4192
Ferrara A. et al., 2022, MNRAS, 512, 58
Ferrara A., Hirashita H., Ouchi M., Fujimoto S., 2017, MNRAS, 471, 5018
Ferrara A., Pallottini A., Dayal P., 2023, MNRAS, 522, 3986
Finkelstein S. L. et al., 2022, ApJ, 940, L55
Fiore F., Ferrara A., Bischetti M., Feruglio C., Travascio A., 2023, ApJ, 943, L27
Fudamoto Y. et al., 2020, MNRAS, 491, 4724
Fudamoto Y. et al., 2023, ApJ, 961, 71
Fudamoto Y., Inoue A. K., Sugahara Y., 2022, MNRAS, 521, 2962
Fujimoto S. et al., 2022, ApJ, 955, 130
Grogin N. A. et al., 2011, ApJS, 197, 35
Hainline K. N. et al., 2023, preprint (arXiv:2306.02468)
Harikane Y. et al., 2020, ApJ, 896, 93
Harikane Y. et al., 2023, ApJS, 265, 5
Hashimoto T. et al., 2018, Nature, 557, 392
Hirashita H., Ferrara A., Dayal P., Ouchi M., 2014, MNRAS, 443, 1704
Hodge J. A., da Cunha E., 2020, R. Soc. Open Sci., 7, 200556
Inami H. et al., 2022, MNRAS, 515, 3126
Inoue A. K., Hashimoto T., Chihara H., Koike C., 2020, MNRAS, 495, 1577
Kennicutt R. C., Evans N. J., 2012, ARA&A, 50, 531
Koekemoer A. M. et al., 2011, ApJS, 197, 36
Laseter I. H. et al., 2023, A&A, 681, A70
Liang L. et al., 2019, MNRAS, 489, 1397
Lower S., Narayanan D., Hu C.-Y., Privon G. C., 2023, preprint (arXiv:2306.07338)
Aravena M., (Feb 2024) The ALMA Reionization Era Bright Emission Line Survey: The molecular gas content of galaxies at z 7 Astronomy & Astrophysics, Volume 682, id.A24, 11 pp., ,
Ma X. et al., 2019, MNRAS, 487, 1844
Madau P., Dickinson M., 2014, ARA&A, 52, 415
Madden S. C. et al., 2020, A&A, 643, A141
Maiolino R. et al., 2023a, preprint (arXiv:2305.12492)
Maiolino R. et al., 2023b, preprint (arXiv:2306.00953)
Matthee J. et al., 2023, preprint (arXiv:2306.05448)
Mennella V., Brucato J. R., Colangeli L., Palumbo P., Rotundi A., Bussoletti E., 1998, ApJ, 496, 1058
Meurer G. R., Heckman T. M., Calzetti D., 1999, ApJ, 521, 64
Morishita T. et al., 2022, ApJ, 947, L24
Naidu R. P. et al., 2022, ApJ, 940, L14
Nakajima K., Ouchi M., Isobe Y., Harikane Y., Zhang Y., Ono Y., Umeda H., Oguri M., 2023, ApJS, 269, 33
Neeleman M. et al., 2021, ApJ, 911, 141
Oesch P. A. et al., 2016, ApJ, 819, 129
Oesch P. A. et al., 2023, MNRAS, 525, 2864
Oesch P. A., Bouwens R. J., Illingworth G. D., Franx M., Ammons S. M., van Dokkum P. G., Trenti M., Labbé I., 2015, ApJ, 808, 104
Rieke M. J., Kelly D., Horner S., 2005, in Heaney J. B., Burriesci L. G., eds, Proc. SPIE Conf. Ser. Vol. 5904, Cryogenic Optical Systems and Instruments XI. SPIE, Bellingham, p. 1
Roberts-Borsani G. et al., 2022, Nature, 7965, 480
Sanders R. L., Shapley A. E., Topping M. W., Reddy N. A., Brammer G. B., 2023, ApJ, 962, 24
Schaerer D. et al., 2020, A&A, 643, A3
Schaerer D., Marques-Chaves R., Barrufet L., Oesch P., Izotov Y. I., Naidu R., Guseva N. G., Brammer G., 2022, A&A, 665, L4
Schouws S. et al., 2023, ApJ, 954, 103
Scoville N. et al., 2017, ApJ, 837, 150
Sommovigo L. et al., 2022, MNRAS, 513, 3122
Sommovigo L., Ferrara A., Carniani S., Zanella A., Pallottini A., Gallerani S., Vallini L., 2021, MNRAS, 503, 4878
Tacchella S. et al., 2022, MNRAS, 522, 6236
Tacchella S. et al., 2023, ApJ, 952, 74
Tacconi L. J. et al., 2018, ApJ, 853, 179
Tacconi L. J., Genzel R., Sternberg A., 2020, ARA&A, 58, 157
Vallini L., Gallerani S., Ferrara A., Pallottini A., Yue B., 2015, ApJ, 813, 36
Williams H. et al., 2023, Science, 380, 416
Witstok J. et al., 2022, MNRAS, 515, 1751
Zanella A. et al., 2018, MNRAS, 481, 1976
Ziparo F., Ferrara A., Sommovigo L., Kohandel M., 2023, MNRAS, 520, 2445

This paper has been typeset from a TEX/LATEX file prepared by the author.